RSC Advances

ROYAL SOCIETY OF CHEMISTRY

www.rsc.org/advances

Study of PTFE–microwave exfoliated Graphene Oxide (MEGO) composites synthesized using low temperature post-irradiation polymerization technique.

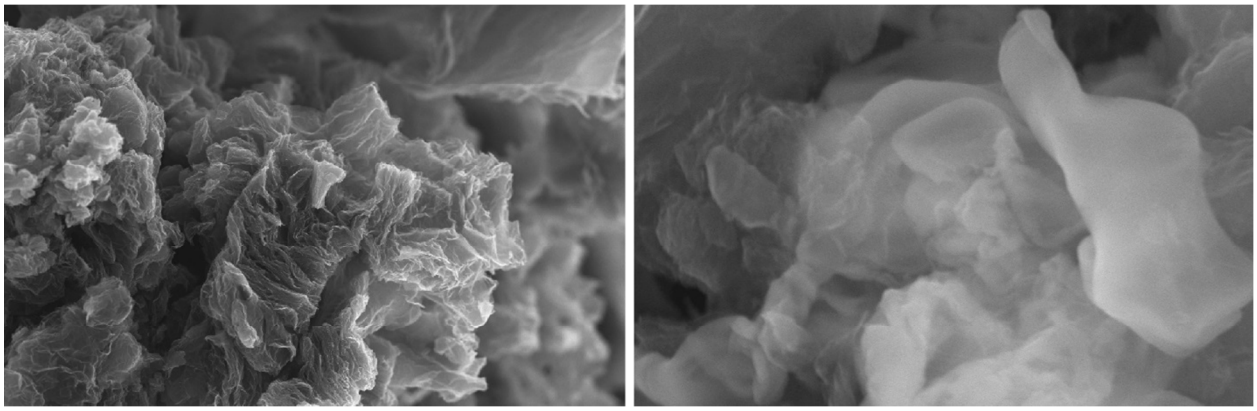

SEM images of MEGO (left) and PTFE-MEGO composite (right)

RSC Advances

RSC Publishing

ARTICLE

POLYMER COMPOSITES PREPARED BY LOW-TEMPERATURE POST-IRRADIATION POLYMERIZATION OF C_2F_4 IN THE PRESENCE OF GRAPHENE-LIKE MATERIAL: SYNTHESIS AND CHARACTERIZATION

Cite this: DOI: 10.1039/xoxxooooox

Received ooth January 2012,
Accepted ooth January 2012

DOI: 10.1039/xoxxooooox

www.rsc.org/

Yury M. Shulga[a,c], Victor N. Vasilets[b], Dmitry P. Kiryukhin[a], Dmitry N. Voylov[d,e], Alexei P. Sokolov[d,e]

Polymer polytetrafluoroethylene (PTFE)–microwave exfoliated graphene oxide (MEGO) composites containing up to 80 wt. % PTFE were prepared by low-temperature post-irradiation polymerization of C_2F_4 in the presence of the graphene-like material. Composites were characterized by FTIR, NMR, XPS, SEM, TGA, XRD, broadband dielectric spectroscopy and DSC techniques. The melting point of PTFE in the composite (332.5°C) was higher than that of pure PTFE by 8.8 °C. The measured values of the melting enthalpy (ΔHm = 51.5 and 45.4 J/g) were used to calculate the extent of crystallinity in PTFE and PTFE–MEGO composite (0.63 and 0.55, respectively). No CF_3 end groups typical of commercial PTFE have been detected in PTFE–MEGO composites.

1. Introduction

Graphene possesses unique electrical and mechanical characteristics [1], and is widely used for modifying polymer properties [2, 3]. However, pure graphene is relatively expensive and hard-to-handle material [4]. In this regard, variety of graphene-like structures which at least partially keep the unique properties of graphene come to the fore [5]. Currently, the large number of polymer composite materials has been obtained using graphene-like structures (GLS). Characteristics of these composites significantly differ from the initial polymer that broadens possible applications [6].

Typically, application of PTFE is often restricted by its low yield strength and high deformability under load. These drawbacks are normally eliminated by addition of strengthening agents. Nevertheless, we found in the literature only several examples of a PTFE/GLS composite [7-10]. Perhaps, the lack of bulk PTFE/GLS composites is due to the fact that the PTFE material is hydrophobic, but the available graphene-like structures, tend to be hydrophilic. In addition, since TFE is a highly reactive compound, its graft polymerization from the gas phase is difficult to perform because of its rapid homopolymerization. But when radiation-induced accumulation of reactive centers is carried out at cryogenic temperatures, the graft polymerization of TFE can be reached practically without formation of homopolymer. γ-Irradiation of sorbent–monomer systems at 77 K gives rise to uniform distribution of reactive centers all over the sorbent surface and hence to uniform post-irradiation graft polymerization, at a markedly lower yield of homopolymer. The technique of low-temperature post-irradiation graft polymerization suggested for TFE [11, 12] may turn helpful in modification of other polymers and inorganic compounds.

Here we report the original method of preparation and characterization of such composites. It has been established that the obtained composites have a number of unusual properties, for example, the synthesized PTFE composites lack CF_3 end groups.

2. Experimental

2.1. Carbon nanomaterial formed upon microwave-assisted exfoliation of graphite oxide (MEGO)

Recently, a conducting material with highly developed surface (s = 3100 m^2/g) has been synthesized [13] from graphite oxide (GO) without extraction of graphene oxide. The synthetic procedure involved the stages of microwave (MW) exfoliation and alkaline activation. But subtle details of these experiments have been described neither in [13] nor in previous paper [14] of the same authors.

Here we will describe our results on the MW treatment of GO films that is accompanied by thermal explosion leading to formation, without alkaline activation, of a conducting carbon material with $s \approx 600$ m^2/g. GO was prepared by using a modified Hummers procedure [15] as described in detail elsewhere [10]. 100 mg GO were mixed with 100 mL water to form a suspension. The suspension was then used to prepare GO films 200–300 μm thick by precipitation onto glass substrates. After mechanical detachment from the substrate, the GO film (around 1 cm^2) was placed into a long silica vessel

clogged with a cotton tissue to catch the products of thermal explosion. Then the vessel was placed into a MW oven (Samsung MC32F604TCT, 2450 MHz, 900 W) and warmed up until thermal explosion of the film.

2.2. Tetrafluorethylene

Commercially available tetrafluoroethylene C_2F_4 (TFE, 0.02% impure) was additionally purified by distillation under reduced pressure.

2.3. Synthesis of nanocomposites by post-irradiation polymerization of C2F4 in the presence of MEGO

Low-temperature post-irradiation polymerization of C_2F_4 in the presence of MEGO was carried out by using two procedures described in [11, 12]. In procedure **1**, MEGO powder was put into a glass cell (~2 cm^3 in volume) and held at 100°C for 2 h to remove adsorbed gases. Then the sample was γ-irradiated at 77°K (Gammatok-100 source, dose 48 kGy, dose rate 0.17 Gy/s). Then TFE was frozen onto the irradiated sample to a MEGO/TFE mass ratio of about 1:20, the cell was sealed and then allowed to slowly (0.6 deg/min) warm-up to room temperature (r.t.), during which the polymerization of TFE took place [11, 12]. The product yield was determined gravimetrically at 23°C after pumping out volatile products.

In procedure **2**, TFE was frozen onto the MEGO powder (degassed at 100°C), the cell was sealed and the MEGO–TFE mixture (1:20 by wt.) was intermixed at r.t. and then γ-irradiated at 77°K.

Since some analyses required larger amounts of product than those formed in a 2-mL cell, we had to perform the described above synthetic procedures 20 times to accumulate a required product batch for each kind of samples.

The commercial PTFE fabricated by suspension polymerization [16] was used as a reference compound.

2.4. Characterization and analytical techniques

2.4.1. C, H, O concentrations and specific surface area

The concentrations of C, H, and O were measured by using an Elementar Vario Cube analyzer. Specific surface area (*s*) was measured by nitrogen absorption method using an Autosorb-1 (Quantachrome Corp.) apparatus. Before surface area measurements, the samples had been subjected to heating in vacuum (10^{-3} torr) at 100°C for 1 h.

2.4.2. NMR spectroscopy

^{19}F NMR spectra were taken at r.t. with an AVANCE 400 (Bruker) solid-state spectrometer. High-resolution spectra were obtained by sample rotation at the magic angle (f = 10 kHz) using standard 90° pulses.

2.4.3. X-ray photoelectron spectroscopy (XPS)

XPS spectra were recorded by using an Axis Ultra DLD (Kratos Analytical Ltd.) spectrometer. Photoemission was excited by monochromatic Al-K_α radiation (E = 1486.7 eV, P = 225 W). The spectra were recorded in a constant transmission mode (160 eV for survey spectra and 20 eV for individual lines). In order to avoid charging of PTFE samples, low-energy excitation was used. Review spectra were taken at a pitch of 1 eV while individual lines, at 0.05 eV. Zone of analysis was about 300 × 700 μm^2 in its size. Residual pressure in the cell compartment did not exceed 10^{-8} torr. The XPS spectra are normally described in terms of the Voigt functions which are a convolution of the Lorentz function (influence of finite lifetime for primary holes) and the Gauss function (instrument response and phonon broadening). However, our experience implies that the use of a simple sum of the Gauss (80%) and Lorentz (20%) functions is sufficient for adequate description of XPS spectra and this approach was used in the present work.

2.4.4. Kinetic calorimetry

These measurements were carried out using the experimental setup described in detail elsewhere [12, 17]. MEGO–TFE samples for kinetic calorimetry were prepared as follows. MEGO powder was placed in a cell (~2 cm^3) and degassed at 373 or 573 K. Then TFE was frozen onto the MEGO powder at 77 K to a MEGO–TFE wt. ratios of 1:30, 1:20, 1:10 and the cell was sealed. The sealed cell was slowly warmed-up to 300 K and held at this temperature for 60 min. With this procedure, TFE was adsorbed to MEGO powder. Then the cell was cooled down to 77 K, put into the calorimeter and the defrosting curve was registered. Since the process was only slightly dependent on MEGO/TFE ratio, the most of results will be presented for MEGO–TFE 1:10 samples.

2.4.5. Differential scanning calorimetry (DSC)

The DSC analysis was performed using a DSC 822 (Mettler-Toledo) instrument. The samples weighting 3–10 mg were placed in aluminum pans with perforated lids under a flow of dry argon (50 mL min^{-1}). The temperature range selected for these measurements was from −30 to +350°C, and the heating rate was 10 deg/min.

2.4.6. Scanning electron microscopy (SEM)

SEM images were taken using a Zeiss LEO SUPRA 25 microscope (electron energy 3–4 kV, inside pressure 1.7 10^{-7} mbar).

2.4.7. Mass spectroscopy

Gaseous products of thermal explosion were analyzed using a MI 1201V mass spectrometer. Ionizing electron beam had the energy of 70 eV. Mass spectra were recorded over the range $1 \leq m/z \leq 250$, where m is atomic mass and z ion charge.

2.4.8. IR spectroscopy

IR spectra were taken at r.t. with a Fourier spectrometer Perkin Elmer Spectrum 100 equipped with a UATR accessory (Ge crystal, n = 4.0) within the range 4000–675 cm^{-1} at a resolution of 4 cm^{-1}.

2.4.7. XRD analysis

A PANalytical X'Pert Pro MRD 4-axis X-ray diffractometer, coupled with a hybrid monochromator and a 0.27◦ parallel plate collimator, was used.

2.4.10. TGA analysis

TA Discovery TGA-MS Thermogravimetric analyzer was used for analyzing thermal decomposition of PTFE-MEGO composites.

2.4.11. Dielectric spectroscopy

Measurements were carried out at ambient conditions on the Novocontrol Alpha-A impedance analyzer (Germany). Conductivity of the samples was calculated using the equation:

$$\sigma = \frac{l}{A} \times \frac{1}{Z}$$

Where σ is conductivity [S/cm], l is the length of sample cylinder [cm], A is the cross section area of the sample cylinder [cm^2], Z is the measured sample impedance [Ohm].

3. Results and discussion

3.1. Characterization of graphite oxide subjected to microwave-assisted exfoliation

Table 1 presents our results on the specific surface (*s*) and surface composition of GO and MEGO samples. Microwave

exfoliation is seen to diminish the amount of O and H but to markedly increase the specific surface of the resultant material.

Table 1. Specific surface (s) and surface composition as calculated from XPS spectra for GO and MEGO samples

	Composition, at. %			*s*, m^2/g
	C	O	H	
GO	50.10	44.81	2.69	20
MEGO	89.95	4.19	0.73	600

The IR spectrum of starting GO is presented in Fig. 1 (curve *1*). Our spectrum agrees with that reported in [18] but exhibits a weaker absorption band at 980–930 cm^{-1} compared to that in [16, 20]. This band is normally assigned to the vibration modes of epoxy group. According to literature data, the overlapping bands in the range 3000–3700 cm^{-1} can be attributed to stretch vibrations of O–H groups; the band at 1730 cm^{-1}, to C=O stretching in carbonyl groups and/or ketones; and the band at 1620 cm^{-1}, to scissor vibrations of water molecules. The nearby band at 1590 cm^{-1} can be attributed to the allowed vibrations of carbon rings within the basal plane. Also the band at 1360–1380 cm^{-1} is normally associated with C–OH vibrations while peaks at 1220–1230 and 1060–1080 cm^{-1}, with the C–O–C and phenyl hydroxyl groups, respectively.

After microwave exfoliation, all the peaks typical for GO disappear from the IR spectrum of MEGO (Fig. 1, curve *2*). We associate this with an increase in the electric conductivity of the sample because curve *2* becomes very similar to the IR spectrum of graphite (curve *3*).

Figure 2 shows the XPS C1*s* spectra in GO and MEGO. The spectrum of C1*s* in GO can be well approximated by three Gaussian curves. According to [21-26], the peak at $E_b \approx 285$ eV can be associated with the carbon atoms that are only surrounded by other carbon atoms. The peak at 287 eV is normally associated with carbon atoms from epoxy (>C–O–C<) and/or hydroxyl (>C–OH) groups while the third peak around 289 eV, to carboxyl groups (–COOH). Judging from the peak intensities, 57% carbon atoms in initial GO are linked with one, and 8% with two oxygen atoms.

The C1*s* spectrum of MEGO markedly differs from that of GO (Fig. 2). Deconvolution results imply (see Fig. 2) that only 15% of carbon atoms in MEGO are linked with one oxygen atom, and 6% are linked with two carbon atoms. Therefore, heat treatment in a microwave oven leads to a significant increase in the fraction of carbon atoms that are not linked with oxygen atoms. Figure 3 shows the SEM images of GO (top image), MEGO (middle image) and MEGO-PTFE (bottom image). After thermal explosion, the planar-parallel particulates of starting GO are seen to get curved, which retains them from collapsing and thus gives rise to a highly developed surface of MEGO. Hence the MW-assisted processing has led to formation of a new conducting material with developed surface.

3.2. Gaseous products formed upon MW-assisted exfoliation of graphite oxide

The data of mass spectrometric analysis suggest (Fig. 4) that the gaseous products contained largely CO (m/z = 28) and CO_2 (m/z = 44). Since for pure CO_2 gas, the peak intensity at m/z = 28 (CO^+ ions) made only about 40% of that at m/z = 44 (CO_2^+ ions), it can be safely assumed that in our case the gaseous products contained 7 CO molecules per 10 CO_2 molecules. The peak at m/z = 18 can be associated with water molecules. The amount of molecular oxygen seems to be insignificant. Unexpected is the presence of SO_2 (m/z = 48, SO^+ ions and m/z = 64, SO_2^+ ions). This can be explained by residual amounts of sulfuric acid used in the preparation of GO. It follows that our MW treatment was also accompanied by purification from sulfuric impurities.

3.3. Calorimetric measurements of polymerization process

Figure 5 presents the calorimetric curves of defrosting for non-irradiated and γ-irradiated 1:10 MEGO–TFE mixtures. They exhibit the *endo* peak of TFE melting around 140 K and the *endo* peak around 240 K associated with some structural transformations in MEGO whose nature is still unclear. Since the monomer adsorbed to MEGO cannot form the crystalline phase at 77 K, only excessive TFE is crystallized, so that the peak at 140 K may correspond to the melting of the above crystals. Using the measured fusion heat and tabulated specific heat of TFE melting (7.5±0.5 kJ/mol), one can estimate the amount of crystallized monomer and hence that of the TFE adsorbed to MEGO. Thus obtained results are collected in Table 2. For γ-irradiated samples (curves 2 in Fig. 5), 22–28% of TFE monomer gets adsorbed to MEGO and do not form a crystal lattice. Accordingly, the sorption-related weight gain of MEGO attained a value of 240–280%. As follows from the Fig. 5b, the heat of TFE fusion in this case decreased by 10–18%. No other thermal effects caused by TFE polymerization were observed until 300 K.

Table 2. Calorimetric and gravimetric results for samples with different initial MEGO/TFE weight ratio (irradiation dose 48 kGr)

#	Initial MEGO/ TFE wt. ratio	Fraction of adsorbed TFE, wt. %	Total PTFE yield, wt. %	PTFE yield from adsorbed TFE, wt. %	MEGO-PTFE composite	
					MEGO/PTFE wt. ratio	PTFE fraction, wt. %
1	1:10.78	26	7.8	22.3	1:0.84	45.6
2	1:10.97	22	8.5	29.5	1:0.93	48
3	1:10.29	25	6.8	19.2	1:0.70	41.1
4	1:9.98	28	8.2	22.1	1:0.82	44.8
5	1:10.34	–	4.7	–	1:0.49	32.9
6	1:10.94	–	0.4	–	1:0.04	3.8
7	1:21.9	–	0.6		1:0.13	11.5

Notes: samples 1-4 obtained by Procedure 2 (see experimental part 2.3.), sample 5 obtained by Procedure 1 but without defrosting, samples 6-7 obtained by Procedure 1

Control experiments have shown that in the absence of MEGO the yield of TFE homopolymer did not exceed 2%, while the total yield of PTFE attained a value of 6.8–8.5% (samples 1–4 in Table 2). Hence the yield of grafted polymer is at least 4.8–6.5%. Therefore, it can be implied that the two processes take place in the system under consideration: (*i*) TFE polymerization in crystals yielding homopolymer of TFE and (*ii*) graft polymerization of the TFE adsorbed to MEGO yielding PTFE–MEGO composite. The data in Table 2 suggest that only 20-30% of adsorbed monomers are polymerized.

The graft polymerization of TFE takes place within the temperature range of monomer melting where the probability for decay of active species also increases. As a result, the

weight gain of MEGO caused by the graft and homo polymerization of TFE attains a value of 70–93%.

Note that for 1:20 and 1:30 mixtures the weight gain in MEGO was 160–185%. It could be expected that an increase in the heating rate (shorter dwell time within the melt zone) would have increased the product yield. But special experiments with sample 1 (Table 2) gave no positive result, as well as preliminary annealing of MEGO at 573 K for several hours to remove gaseous products and water (sample 4, Table 2).

A necessary condition for effective graft polymerization is the adsorption of monomer to MEGO. This is confirmed by experiments with sample 5 (Table 2): TFE was frozen onto MEGO at 77 K and subjected to γ-irradiation without defrosting. In this case the conditions for adsorption were less favorable (compared to samples 1–4) and the yield of polymer turned out lower (Table 2) by a factor of two.

Similar results were obtained with samples 6 and 7 (Table 2). In these experiments, MEGO powder was degassed at 373 K, irradiated at 77 K, and non-irradiated TFE was frozen onto irradiated MEGO at 77 K, without intermixing. As a result, the TFE conversion was only 0.4–0.6%, while the weight gain in MEGO did not exceed 13%.

The above results suggest that the TFE monomers adsorbed to the surface of the pores formed in MEGO do not undergo crystallization and exhibit higher polymerizability than in its own crystal matrix. Joint irradiation of 1:10 MEGO–TFE mixtures leads to formation of the composite containing around 45% PTFE (Table 2). In case of 1:20 or 1:30 mixtures, the weight gain in MEGO is 165–180%, the weight fraction of PTFE being 62–65%, respectively.

3.4. IR spectra of MEGO–PTFE composites

The IR spectra of PTFE are well known [27]. The strongest bands are associated with symmetrical and anti-symmetrical stretching modes of the C–F bond in the $–CF_2–$ unit. For the polymer obtained by low temperature post irradiation polymerization these bands are at 1206 and 1151 cm^{-1} (Fig. 6, curve *1*). The weaker bands 1714 and 1786 cm^{-1} belonging to the groups with middle and terminal C=C bonds in linear polymer chain are typical of irradiated perfluorocarbons [28]. The C=C bonds at chain branching show absorption at lower wave numbers (1670 cm^{-1}) [28]. We failed to detect the bands of $–CF_3$ terminal groups around 980 cm^{-1}. It can thus be concluded that in our polymer terminal are the $–CF=CF_2$ groups (1786 cm^{-1}).

The IR spectrum of the composite (curve *2*) does not show the presence of signal from terminal $–CF=CF_2$ groups (1786 cm^{-1}). This is in line with the results of our XPS measurements (see paragraph 3.5. below) showing that in PTFE the terminal group represents an oxygen bridging group linked to a carbon matrix. The IR spectra of our composites prepared upon joint irradiation of MEGO–TFE and separate irradiation of TFE were essentially the same.

3.5. XPS results for MEGO–PTFE composites

In this section, our MEGO–PTFE composites will be analyzed in comparison with starting MEGO and PTFE. The XPS spectra and quantum-chemical calculations clearly imply that the perfluoroalkyl chains of PTFE are linked to MEGO via the hydroxyl groups of MEGO.

The survey XPS spectrum of MEGO (Fig. 7, curve *1*) shows the presence of carbon, oxygen, and sulfur. Surface-layer compositions of our composites as derived from integral intensity of XPS spectral bands are presented in Table 3.

Table 3. Surface-layer compositions as derived from XPS spectra

Sample	Content, at. %			
	C	O	F	S
MEGO	86.3	12.9	0	0.7
Composite 1*	87.6	11.7	0.4	0.3
Composite 2**	61.2	8.9	29.6	0.3
PTFE	32.2	0.0	67.8	0.0

** Composite 1 was obtained by procedure **1** at a MEGO weight increment of 12.5%.*

*** Composite 2 was obtained by procedure **2** at a MEGO weight increment of 185%*

The presence of sulfur can be associated with sulfuric residuals left after synthesis of GO according to Hummers [15]. Our carbon fractions agree with the results of our elemental analysis, although the XPS results for oxygen are overestimated (4.2-fold) tentatively because of prolonged storage of samples in air. Comparing MEGO and composite 1 (Table 3), we may conclude that γ-irradiation results in insignificant oxygen losses and partial reduction of GO, which could be readily expected. As is known [29], the UV photolysis of GO yields water and carbon oxides. The presence of trace amounts of fluorine in composite 1 (Table 3) suggests that the polymerization of C_2F_4 under the action of γ-irradiated MEGO practically does not occur. This is indicative of short lifetimes of radiation-induced reactive species capable of starting-up the polymerization process. But when monomer is already present during irradiation, the situation changes drastically: the F content of composite 2 attains a value of around 30 at. % (Table 3). Comparing the C:O ratios for MEGO and composite 1 and 2, one can note that they are similar (6.7:1 and 7.5:1), while upon deduction of PTFE carbon (i.e. ~15%) for composite 2 this ratio becomes equal to 5.2:1. So the O content of composite 2 is higher than that of starting MEGO.

Figure 8 shows the high-resolution XPS spectra of C1*s* in MEGO, composite 1, and composite 2. Similarity of spectra *1* and *2* clearly indicates that γ-irradiation in the absence of TFE has no influence on chemical environment of MEGO. Both spectra also exhibit a shoulder around 285.5 eV. In view of their asymmetry (Doniach–Šunjić spectral lines [30]), these bands cannot be approximated by two Gaussian or Lorentzian functions. Tentatively, this asymmetry can be associated with high conductivity of MEGO, as in the case of graphite [31].

Spectrum *3* in Fig. 8 exhibits an additional band peaked at 291.3 eV typical of PTFE [32] and a shoulder marked with an asterisk. Origin of this shoulder still remains unclear. When spectrum *1* was subtracted from spectrum *3*, the shoulder had acquired a shape of the band peaked at 282 eV (see Fig. 8), which can be attributed to carbon atoms with a small negative charge, as in transition metal carbides [32].

Spectrum *3* also exhibits a broad band at 291.3 eV. Its half-width at half maximum (HWHM), 1.84 eV, is greater than that for high-molecular PTFE (0.90 eV) measured under similar conditions. This can be regarded as an evidence for structure imperfection of the polymer formed at low temperatures. This is also supported by the XPS F1*s* spectra of composite 2 and PTFE presented in Fig. 9. The HWHM for the band of composite 2 (2.16 eV) also is markedly broader than that for PTFE (1.28 eV). The influence of non-uniform charging of polymer globules can also be excluded since the band position

and HWHM were independent of duration and intensity of probing X-ray beam. Interesting information can be inferred from the XPS O1*s* spectra (Fig. 10). The spectrum of initial MEGO (Fig. 10, curve *1*) exhibits two bands peaked at 533.4 and 531.3 eV. According to [33-40], the main oxygen-containing groups in the oxides of graphite and graphene are hydroxyl (C–O–H) and epoxy (C–O–C) groups. In the O1*s* spectra, they manifest themselves as a band peaked around 533 eV [38, 41], while the band at 531 eV is associated with a carbon atom of the C=O bond. In the spectrum of composite 1 (Fig. 10, curve *2*), the band intensity at 533.4 eV becomes relatively stronger. But in the spectrum of composite 2 (Fig. 10, curve *3*) there appears a new band with a maximum at 530.6 eV and all three peaks acquire the same amplitude. This peak can hardly be assigned to radiation-induced oxygen-containing groups in MEGO simply because this band is absent in the spectrum of composite 1 (Fig. 10, curve *2*). So it seems reasonable to associate this peak with the presence of PTFE. Since the oxygen concentration on the PTFE surface is close to zero, it can be assumed that the perfluoroalkyl fragments become linked with oxygen atoms of MEGO during polymerization, via formation of C(MEGO)–O–CF_2R_F bridging groups between the polymer chain and the graphene sheet. In such a case, we would be able to explain the larger HWHM of the F1s peak in the spectrum of composite 2 (see Fig. 9).

The above results suggest that the low-temperature polymerization of TFE proceeds with participation of short-lived oxygen atoms formed upon radiation-assisted destruction of hydroxyl groups in MEGO. Thus prepared PTFE differs from normal high-molecular PTFE by retained links with the nanocarbon matrix (at low PTFE concentrations). This link suppresses crystallization of the polymer. Indeed, commercial PTFE is comprised of lamellar crystalline structures. In our case (see below), the crystallinity of PTFE in composites is lower than that in normal PTFE.

3.6. ^{19}F NMR spectra

The samples used in ^{19}F NMR measurements are characterized in Table 4. The spectrum of composite 1 (Fig. 11) represents a single-line signal from CF_2 with a chemical shift of –123 ppm (with respect to $CClF_3$) along with two satellites. No signals from terminal $–CF_2–CF_3$ or $–CF=CF_2$ groups [42] were observed. Hence it can be assumed that the terminal groups of PTFE are linked with MEGO. As reported previously [12], the role of polymerization centers was played by oxygen atoms.

Table 4. Composites used in ^{19}F NMR measurements

	MEGO/TFE wt. ratio	MEGO wt. increment, %	Consumed TFE, %
Composite 1	1 : 20	185	8.3
Composite 2	1 : 30	140	4.4

The present results give grounds to assume that the chain termination process occurs via involvement of the reactive sites of the graphene material under study.

The spectrum of composite 2 is rather similar (see Fig. 11) and become identical with that of composite 1 when normalized to equal peak heights. This is indicative of similar surrounding but different amounts of F atoms in both materials.

Therefore, the NMR data suggest our composite is comprised of the fluorocarbon chains whose ends are attached to the carbon matrix of MEGO. This is evidenced by the absence of terminal groups typical of conventional PTFE.

3.7. TGA analysis

To analyze decomposition temperature of PTFE-MEGO composites thermogravimetric analysis was used. The results for five samples with MEGO content from 0 to 60 wt. % are presented in the Table 5. The decomposition temperatures were defined by the maximum on the temperature dependence of the weight loss derivative. It is noticeably that they increased with MEGO concentration (see Fig. 12). The maximal increase of the decomposition temperature detected for 67.13 wt. % of MEGO. The MEGO contents were determined from the residue in the TGA curves at 1000 °C.

Table 5. Weight fraction of MEGO in composites and decomposition temperatures of MEGO/PTFE

Sample #	Weight fraction of MEGO, wt. %	Weight fraction of PTFE, wt. %	Decomposition temperature, °C
0	0	100	591-592
I	2.92	97.08	593
II	10.71	89.29	597
III	23.16	76.84	606
IV	67.13	32.87	608

3.8. XRD analysis

Figure 13 shows several X-ray diffraction spectra of different specimens (MEGO, PTFE and MEGO/PTFE (**III**)). It can be seen from the figure that adding MEGO to the PTFE has visibly changed peak intensity (at $2\theta \approx 18^{o}$), which is typically associated with PTFE crystalline structure [43]. However, it should be confirmed by decreasing of amorphous PTFE [43], which was undetectable in our case due to overlapping with MEGO broad maximum [44].

3.9. DSC curves

For ideal PTFE crystals the melting point (T_m) is 327°C [41] but may vary depending on material state, prehistory, irradiation dose, etc. [45-47]. In this context, DSC testing of new PTFE-containing composite materials around T_m becomes exceedingly important. This technique can also be used to determine the mean molecular weight of PTFE [46].

Figure 14 presents the DSC curves for the PTFE obtained by low-temperature polymerization and MEGO–PTFE composite 2 from Table 3. For PTFE and MEGO–PTFE composite melting points T_m are seen to be 323.7 and 332.5°C, respectively. Note that for melting, the HWHM of this phase transition in the composite is twice narrower than in the polymer. This can be associated with a narrower molecular weight distribution for the composite. The enthalpy of melting (ΔH_m) makes a value of 51.5 and 29.4 J/g for the polymer and composite, respectively. After correction for 65% TFE in composite 2 (Table 3), for composite we obtained $\Delta H_m = 45.4$ J/g.

When $5\cdot10^5 < M_n < 5\cdot10^7$, then according to [48], the following expression must hold true: $M_n = 2.1\cdot10^{10}\ \Delta H_m^{-5.16}$, where ΔH_m is expressed in cal/g. From this formula, we obtained M_n as $5.0\cdot10^4$ and $9.8\cdot10^4$ for the polymer and composite,

respectively. Although beyond the applicability limits for the above expression [48], it seems safe to conclude that the low-temperature polymerization yields polymers with a number of –CF_2– chain links much below 10 000. In the presence of graphene material, the average length of a polymer chain becomes larger.

The extent of crystallinity (x_c) for our materials can be estimated by using the formula: $x_c = \Delta H_m/\Delta H_m^{\infty}$, where ΔH_m^{∞} is the enthalpy of melting for crystalline PTFE. According to [49, 50], for PTFE ΔH_m^{∞} = 82 J/g. Using the above values of ΔH_m (51.5 and 45.4 J/g), for x_c we obtain 0.63 and 0.55 for the polymer and composite, respectively.

A low-temperature phase transitions around 7.8 and 13.1°C (with ΔH_m 3.7 and 1.2 J/g, Fig. 14) can be regarded [49] as part of the overall melting process.

3.10. Dielectric spectroscopy measurements

Dielectric spectroscopy in a wide frequency range (from 10^{-1} to 10^7 Hz) was employed to measure conductivity and relaxation properties of MEGO and prepared composites. MEGO-PTFE composites with MEGO fraction less than 3% did not show any difference in a relaxation and conductivity (below measurement range $>10^{-20}$ S/cm) behavior in comparison to pure PTFE at room temperature (T=20°C). Above this concentration, conductivity reached constant and frequency undependable value of about 10^{-3} S/cm due to percolation effect (Fig. 15). As a result, high conductivity hindered a study of relaxation properties.

Conclusions

The melting of the TFE (140 K) mixtures with MEGO that were preliminary γ-irradiated at 77 K was found to result in a formation of the PTFE–MEGO composite containing 30–80% PTFE. We characterized composites and PTFE prepared in the absence of MEGO using solid-state NMR (rotation at a magic angle), DSC, XPS, FTIR, SEM, TGA, XRD and broadband dielectric spectroscopy. We estimated the mean chain lengths for both pure polymer and composite and found that in the presence of graphene material it becomes larger. The XPS spectrum of O1s in the composite contained additional peak corresponded to a bridging oxygen atom between the graphene sheet and carbon atom of the polymer chain indicating chemical interaction. Using DSC data analysis we found that a necessary condition for graft polymerization was the adsorption of monomer to substrate and joint irradiation of TFE and MEGO below melting point of TFE.

The composites may turn promising for use in fabrication of machine parts with elevated yield strength and improved wear resistance as compared to those made out of conventional PTFE. The study of mechanical properties will be pursued in the next work.

Acknowledgements

This work was partially supported by the Russian Foundation for Basic Research (project nos. 12-03-00261 and 13-03-00398) and RF Ministry of Education and Science (State Contract No. 14.594.21.0007, RFMEFI59414X0007), State Assignment No. 11.1797.2014/K. US team thanks the Division of Materials Sciences and Engineering, DOE Office of Basic Energy Sciences for financial support.

Notes and references

[a] Institute of Problems of Chemical Physics, Russian Academy of Sciences, Chernogolovka, Moscow region, 142432, shulga@icp.ac.ru

[b] Institute for Energy Problems in Chemical Physics, Russian Academy of Sciences, Chernogolovka, Moscow region, 142432

[c] National University of Science and Technology MISIS, Leninsky pr. 4, Moscow 119049, Russia

[d] Department of Chemistry, University of Tennessee, Knoxville, TN, USA 37916-1600

[e] Chemical Sciences Division, Oak Ridge National Laboratory, Oak Ridge, TN, USA 37830

† Footnotes should appear here. These might include comments relevant to but not central to the matter under discussion, limited experimental and spectral data, and crystallographic data.

Electronic Supplementary Information (ESI) available: [details of any supplementary information available should be included here]. See DOI: 10.1039/b000000x/

References

1. C. Lee, X. Wei, J.W. Kysar, et al, *Science*. 2008, **321**, 385.
2. T. K. Das and S. Prusty, *Polymer-Plastics Tech. and Eng.*, 2013, **52**, 319
3. T. Kuila, S. Bhadra, D. Yao et al, *Prog. Polym. Sci.*, 2010, **35**, 1350.
4. D. R. Dreyer, S. Park, C. W. Bielawski et al. *Chem. Soc. Rev.*, 2010, **39**, 228
5. D.A. Dikin, S. Stankovich, E.J. Zimney, et al, *Nature.* 2007, **448**, 457.
6. J. Du, H. Cheng, *Macromol. Chem. Phys.* 2012, **213**, 1060
7. S. S. Kandanur, M. A. Rafiee, F. Yavari, et al, *Carbon.* 2012, **50**, 3178
8. R. K. Goyal, M. Yadav, *J. Appl. Polym. Sci.* 2013, **127**, 3186
9. T. Huang, T. Li, Y. Xin, *RSC Adv.* 2014, **4**, 19814
10. V.E. Muradian, M.G. Ezernitskaya, V.I. Smirnova, et al, *Zh. Obshch. Khim.* 1991, **61**, 2626.
11. A.A. Davranov, D.P. Kiryukhin, M.R. Muitdinov, et al, *High Energ. Chem.* 1998, **22**, 423.
12. D.P. Kiryukhin, *High Energ. Chem.* 2011, **45**, 165.
13. Y. Zhu, S. Murali, M.D. Stoller, et al. *Science*. 2011, **332**, 1537.
14. Y. Zhu, S. Murali, M.D. Stoller, et al, *Carbon*. 2010, **48**, 2118.
15. W.S. Hummers, R.E. Offeman, *J. Am. Chem. Soc*. 1958, **80**, 1339.
16. T.J. Romack, B.E. Kipp, J.M. DeSimone, *Macromolecules*. 1995, **28**, 8432.
17. I. M. Barkalov, D. P. Kiryukhin, *Int. Rev. Phys. Chem*. 1994, **13**, 337.
18. Y. Si, E.T. Samulski, *Nano Lett*. 2008, **8**, 1679.
19. H.-K. Jeong, Y.P. Lee, M.H. Jin, et al., *Chem. Phys. Lett*. 2009, **470**, 255.
20. L.J. Cote, R. Cruz-Silva, J Huang, *J. Am. Chem. Soc.* 2009, **131**, 11027.
21. T. Szabo, O. Berkesi, P. Forgo, et al, *Chem. Mater*. 2006, **18**, 2740.
22. J.R. Lomeda., C.D. Doyle, D.V. Kosynkin, et al., *J. Am. Chem. Soc*. 2008, **130**, 16201.
23. C. Xu., X. Wang., J. Zhu, *J. Phys. Chem. C*. 2008, **112**, 19841.

24. S. Park, K-S. Lee, G Bozoklu, et al, *ACS Nano*. 2008, **2**, 572.
25. J.I. Paredes, S. Villar-Rodil, P. Solis-Fernandez, et al, *Langmuir*. 2009, **25**, 5957.
26. C. Shan, H Yang, J. Song, et al, *Anal. Chem*. 2009, **81**, 2378.
27. S. Krimm, *Fortschr. Hochpolym. Forsch*. 1960, **2**, 51.
28. A. Oshima, S. Ikeda, E. Katoh, et.al, *Radiat. Phys. Chem*. 2001, **62**, 39.
29. Y.M. Shulga, V.M. Martynenko, V.E. Muradyan, et al, *Chem. Phys. Lett.* 2010, **498**, 287.
30. S. Doniach, M. Šunjić, *J. Phys. C*. 1970, **3**, 285.
31. J.A. Leiro, M.H. Heinonen, T. Laiho et al, *J. Electron Spectrosc. Relat. Phenom*. 2003, **128**, 205.
32. V.I. Nefedov, X-ray electron spectroscopy of chemical compounds. Khimiya: Moscow, 1984: pp 1-255.
33. R. Larciprete, S Fabris, T. Sun, et al, *J. Am. Chem. Soc.* 2011, **133**, 17315.
34. A. Barinov, O. B. Malcioglu, S. Fabris, et al, *J. Phys. Chem. C.* 2009, **113**, 9009.
35. R. Larciprete, S. Gardonio, L. Petaccia, et al, *Carbon*. 2009, **47**, 2579.
36. N.A. Vinogradov, K. Schulte, M.L. Ng, et al, *J. Phys. Chem. C*. 2011, **115**, 9568.
37. D. Yang, A. Velamakanni, G. Bozoklu, et al, *Carbon*. 2009, **47**, 145.
38. C. Kozlowski, P.M.A. Sherwood, *J. Chem. Soc. Faraday Trans. I*. 1984, **80**, 2099.
39. M.I. Awad., M.M. Saleh, T. Ohsaka, *J. Solid. State Electrochem.* 2008, **12**, 251.
40. G. Zhang, S. Sun, D. Yang, et al, *Carbon*. 2008, **46**, 196.
41. C. Mattevi, G. Eda, S. Agnoli, et al, *Adv. Funct. Mater*. 2009, **19**, 2577.
42. J.S. Forsythe, D.J.T. Hill, S Mohajerani, et al, *Radiat. Phys. Chem*. 2001, **60**, 439.
43. G. Deli, Z. Bing, X. Qun-Ji, et al, *Wear*, 1990, **137**, 25
44. D. Antiohos, K. Pingmuang, M.S. Romano, et al, *Electrochimica Acta* 2013, **101**, 99
45. Y.P. Khanna, G. Chomyn, R. Kumar, et al, *Macromolecules*. 1990, **23**, 2488.
46. Y.P. Khanna, J. Mater. *Sci. Lett*. 1988, **7**, 817.
47. A. Oshima, Y. Tabata, H. Kudoh, et al, *Radiat. Phys. Chem*. 1995, **45**, 269.
48. T. Suwa, M. Takehisa, S. Machi, *J. Appl. Polym. Sci.* 1973, **17**, 3253.
49. R. Androsch, B. Wunderlich, H.-J. Radusch, *J. Therm. Anal. Calorim*. 2005, **79**, 615.
50. J. Runt, L. Jin, S. Talibuddin, C.R. Davis, *Macromolecules*. 1995, **28**, 2781.

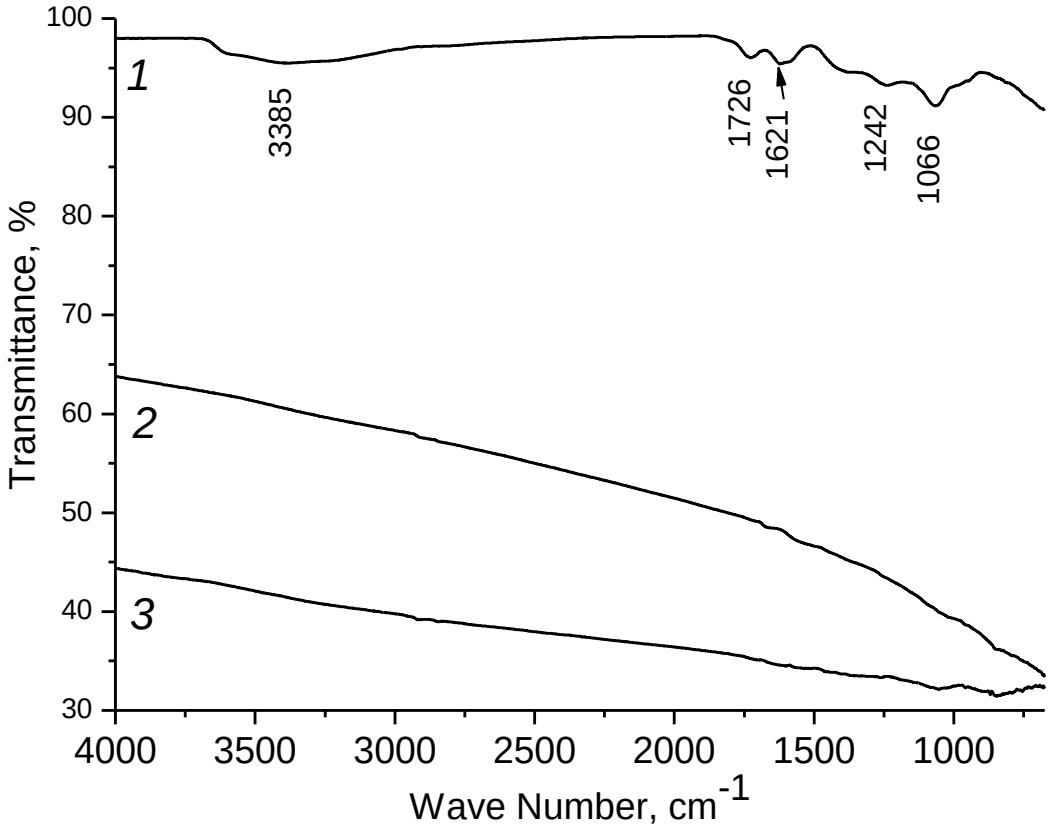

Fig. 1. IR spectra of GO (*1*), MEGO (*2*), and graphite (*3*).

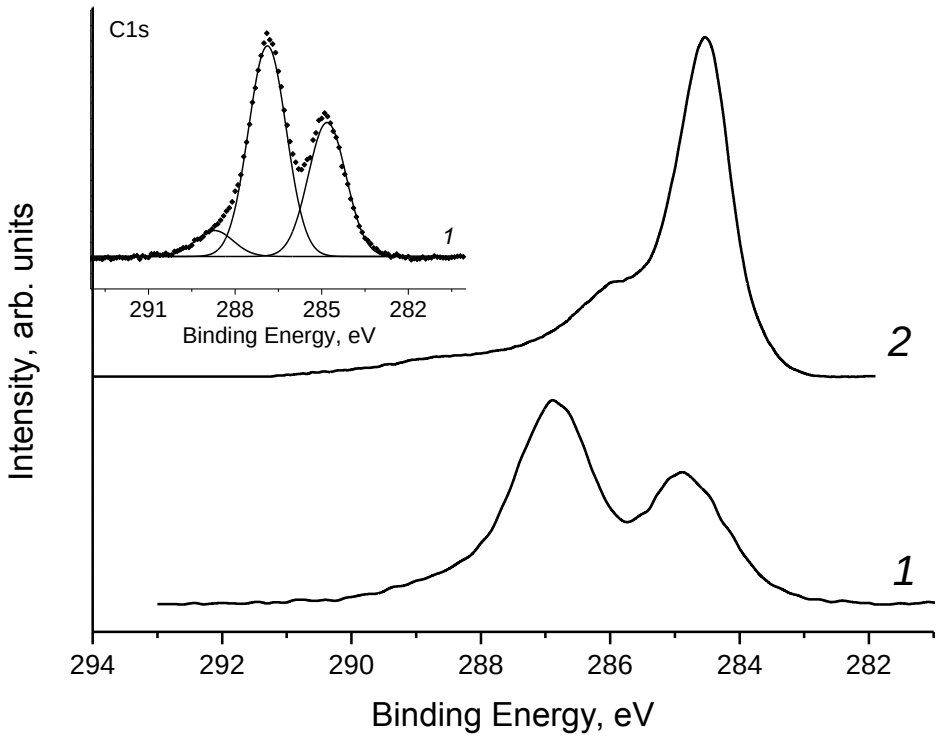

Fig. 2 XPS C1s spectra of GO (*1*) and MEGO (*2*). Inset: fitting of spectrum *1* by Gaussians.

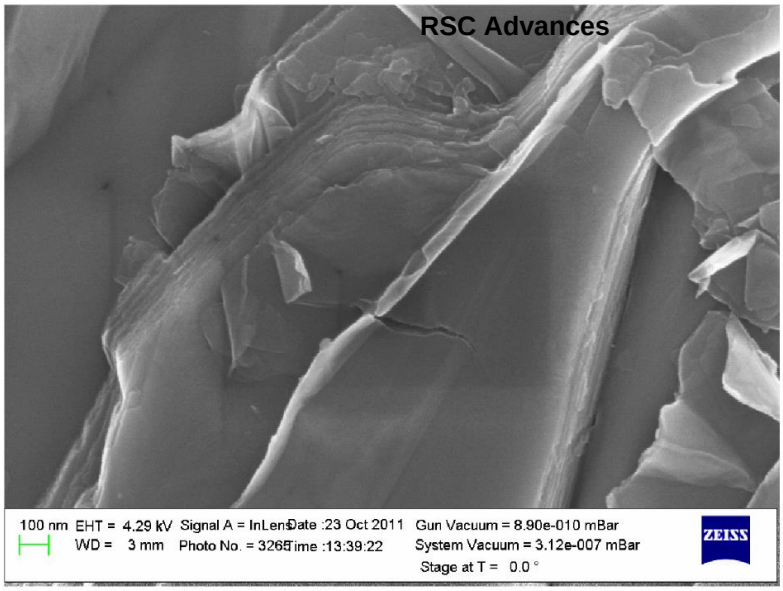

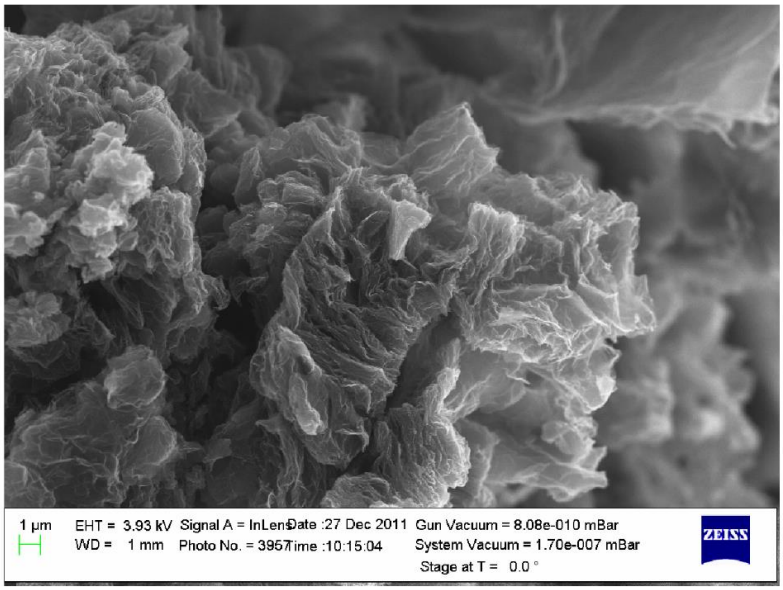

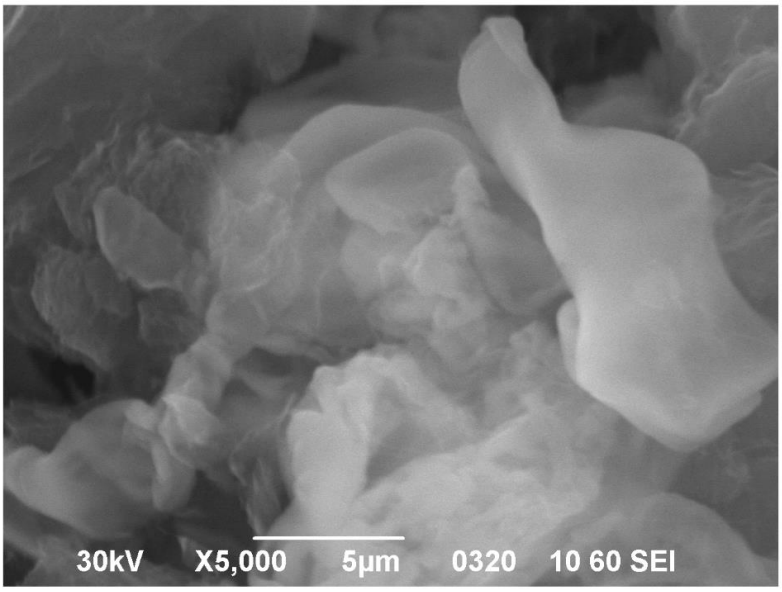

Fig. 3. SEM images of GO (top image), MEGO (middle image) and MEGO-PTFE (bottom image)

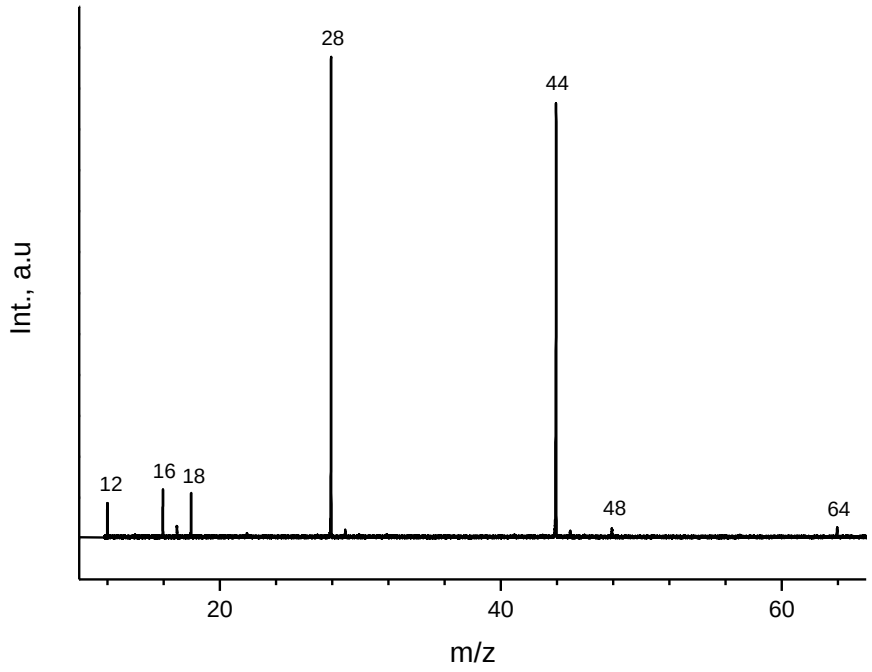

Fig. 4. Mass spectra of gaseous products formed upon MW-assisted thermal explosion of GO film in vacuum.

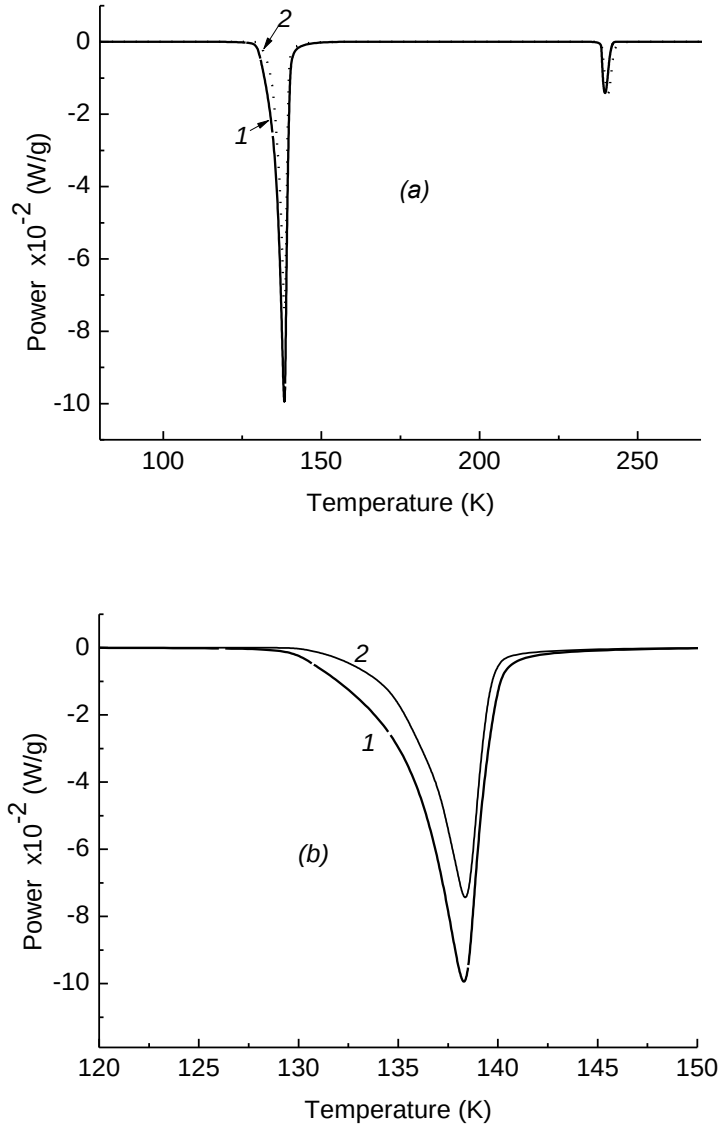

Fig. 5. (a) Calorimetric curves of defrosting for (*1*) non-irradiated and (*2*) γ-irradiated 1 : 10 MEGO–TFE mixtures (irradiation dose 48 kGr) and (b) zoom of curves *1* and *2*.

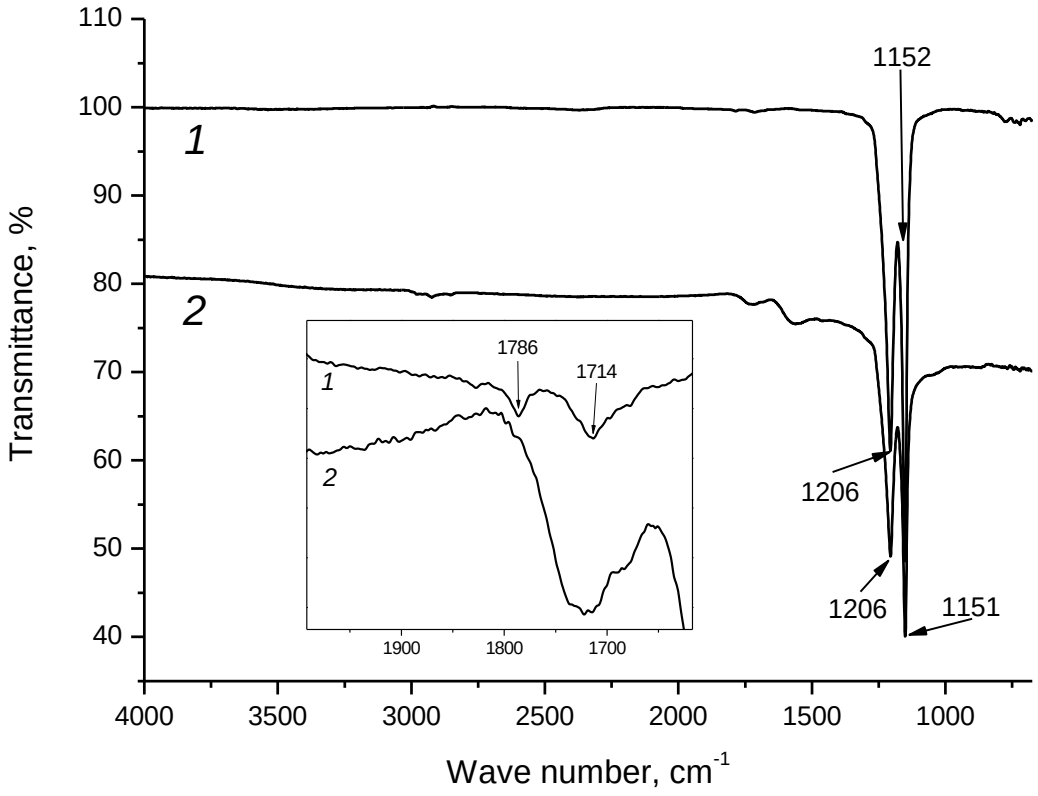

Fig. 6. IR spectra of PTFE (*1*) and MEGO–PTFE composite (*2*). PTFE samples were prepared by low-temperature post-irradiation polymerization of TFE.

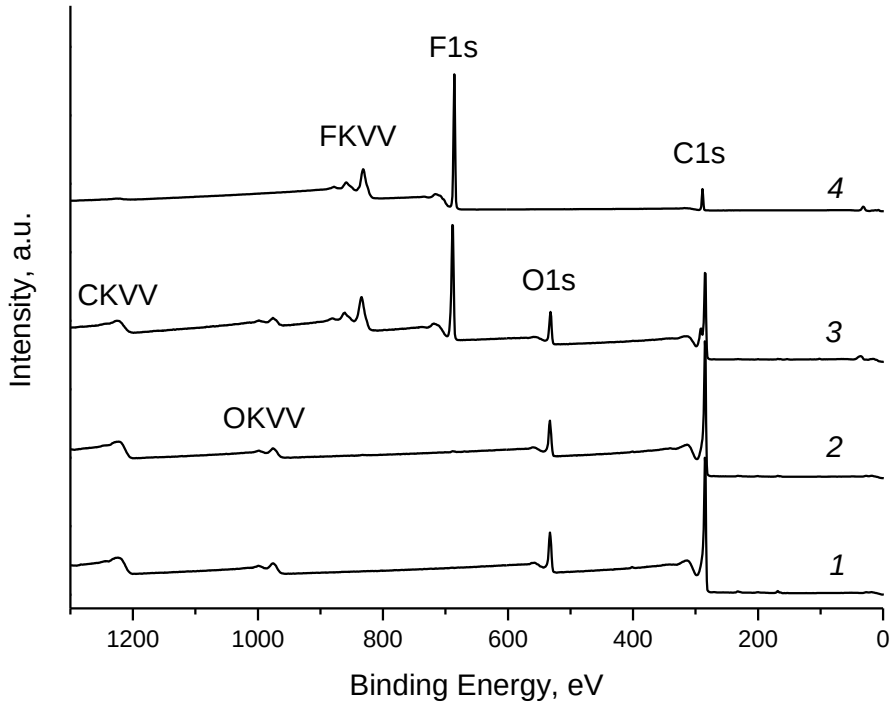

Fig. 7. Survey XPS spectra of MEGO (*1*), composite 1 (*2*), composite 2 (*3*), and PTFE (*4*).

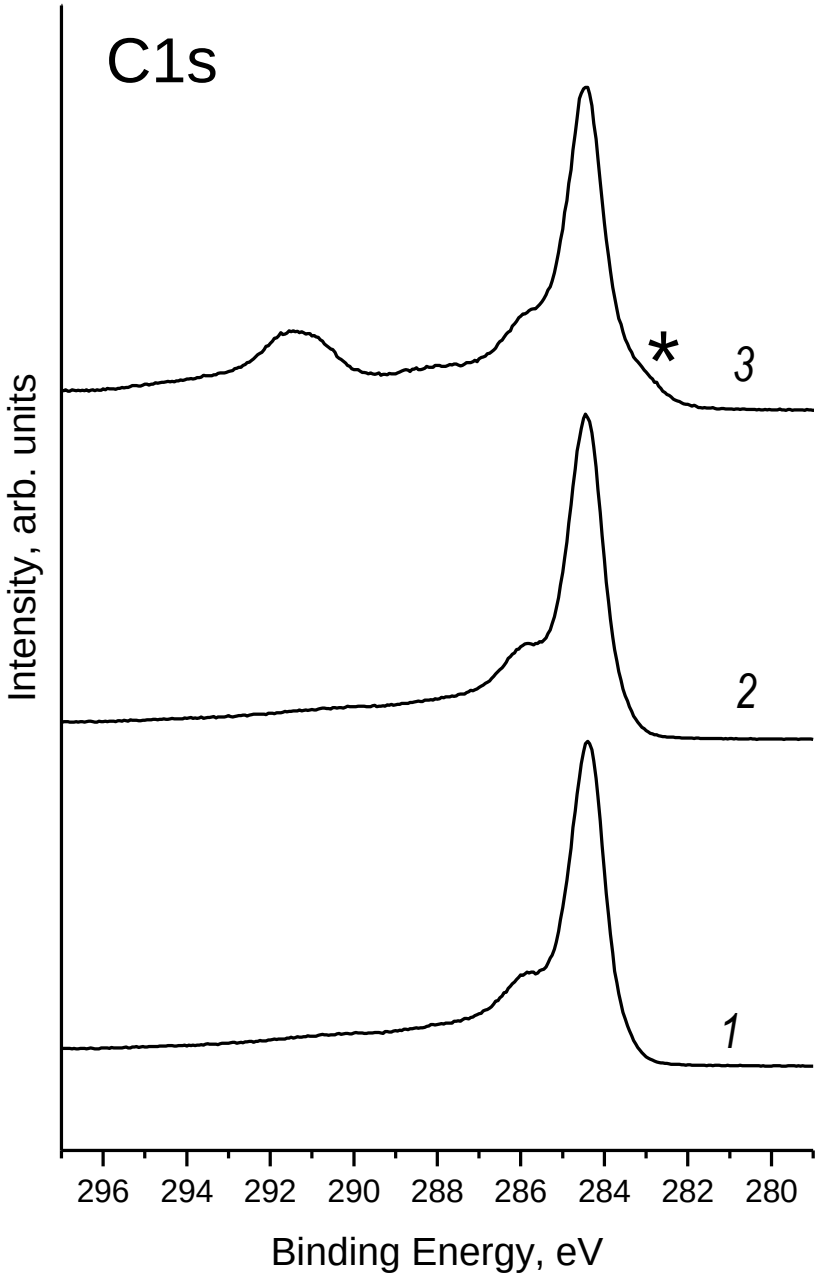

Fig. 8. High-resolution XPS spectra of C1s of MEGO (*1*), composite 1 (*2*), and composite 2 (*3*) (cf. Table 3).

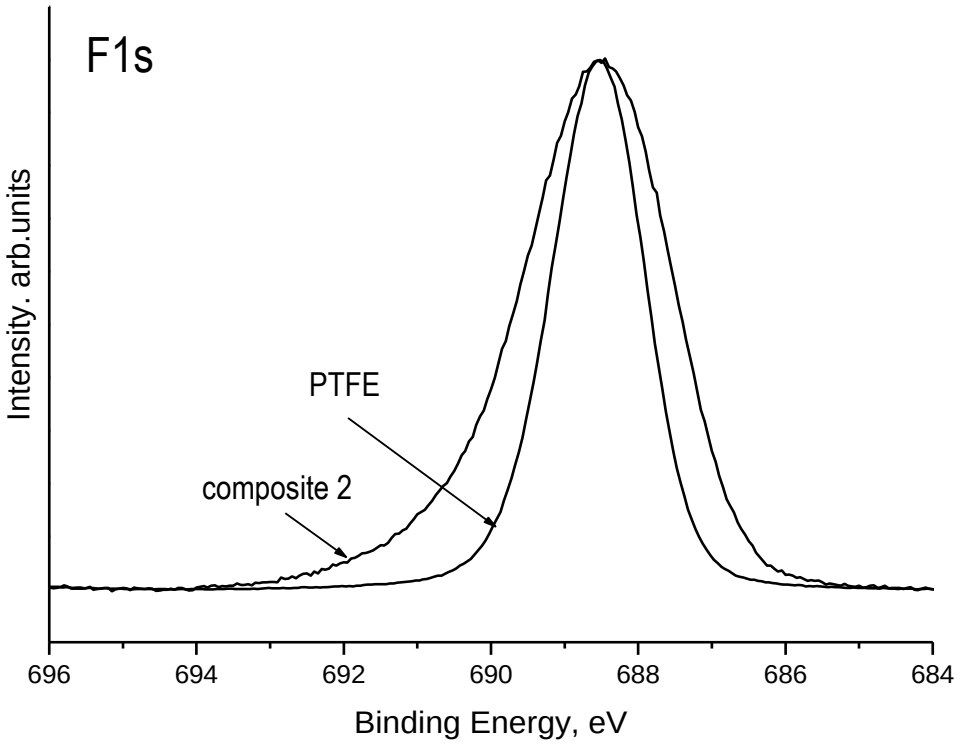

Fig. 9. High-resolution XPS spectra of F1s in composite 2 (cf. Table 3) and PTFE.

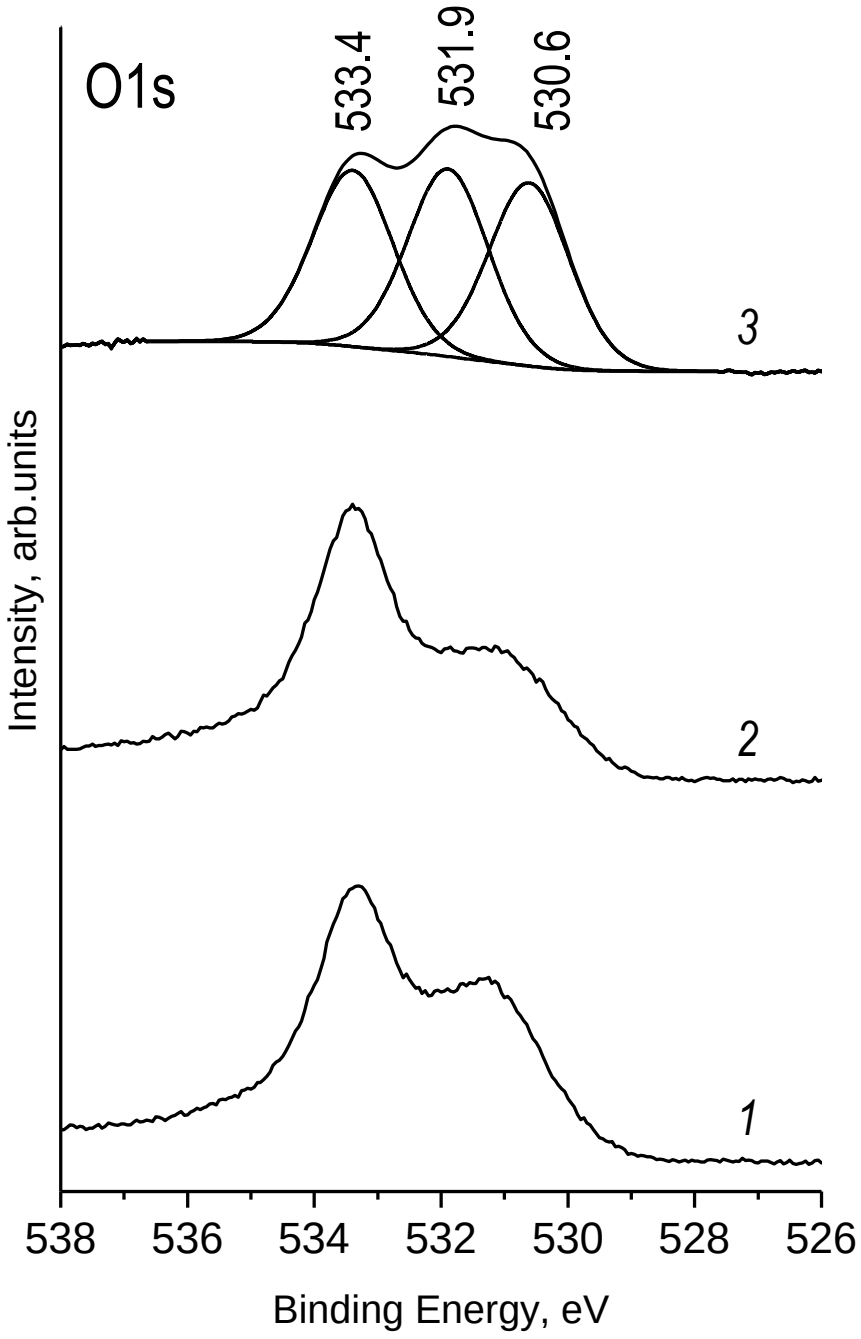

Fig. 10. High-resolution XPS spectra of O1s in starting MEGO (*1*), composite 1 (*2*), and composite 2 (*3*) (for nomenclature see Table 3).

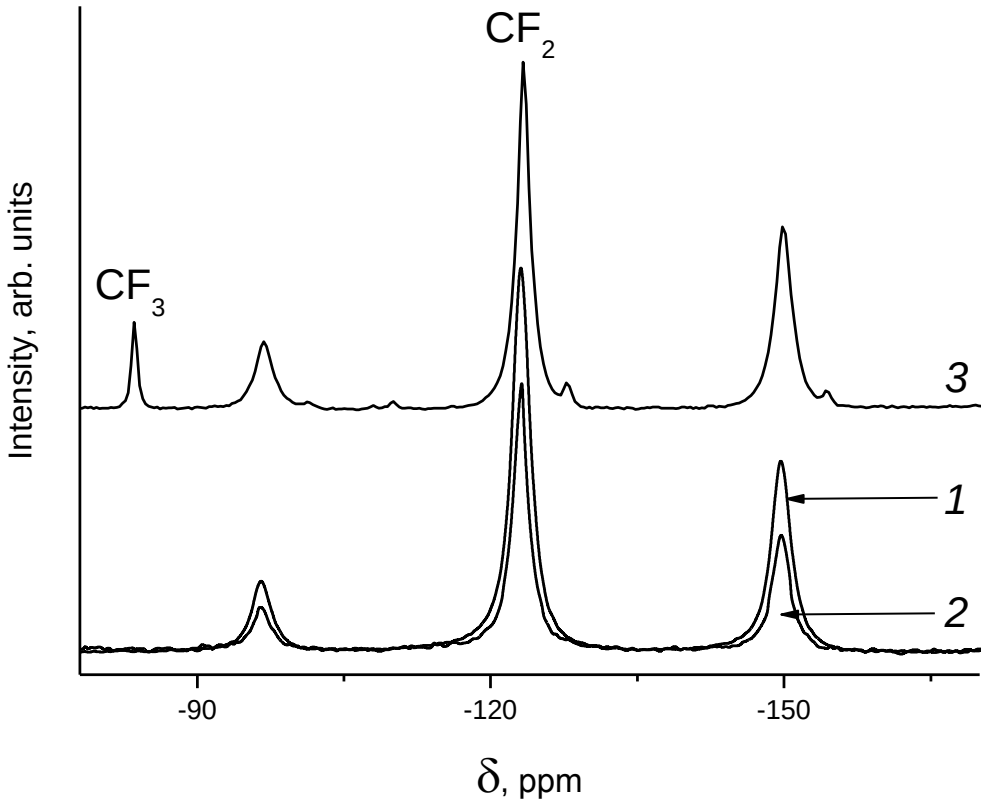

Fig. 11. High-resolution ^{19}F NMR spectra of composites **I** (*1*), **II** (*2*) (for details see Table 4) and commercial PTFE (*3*).

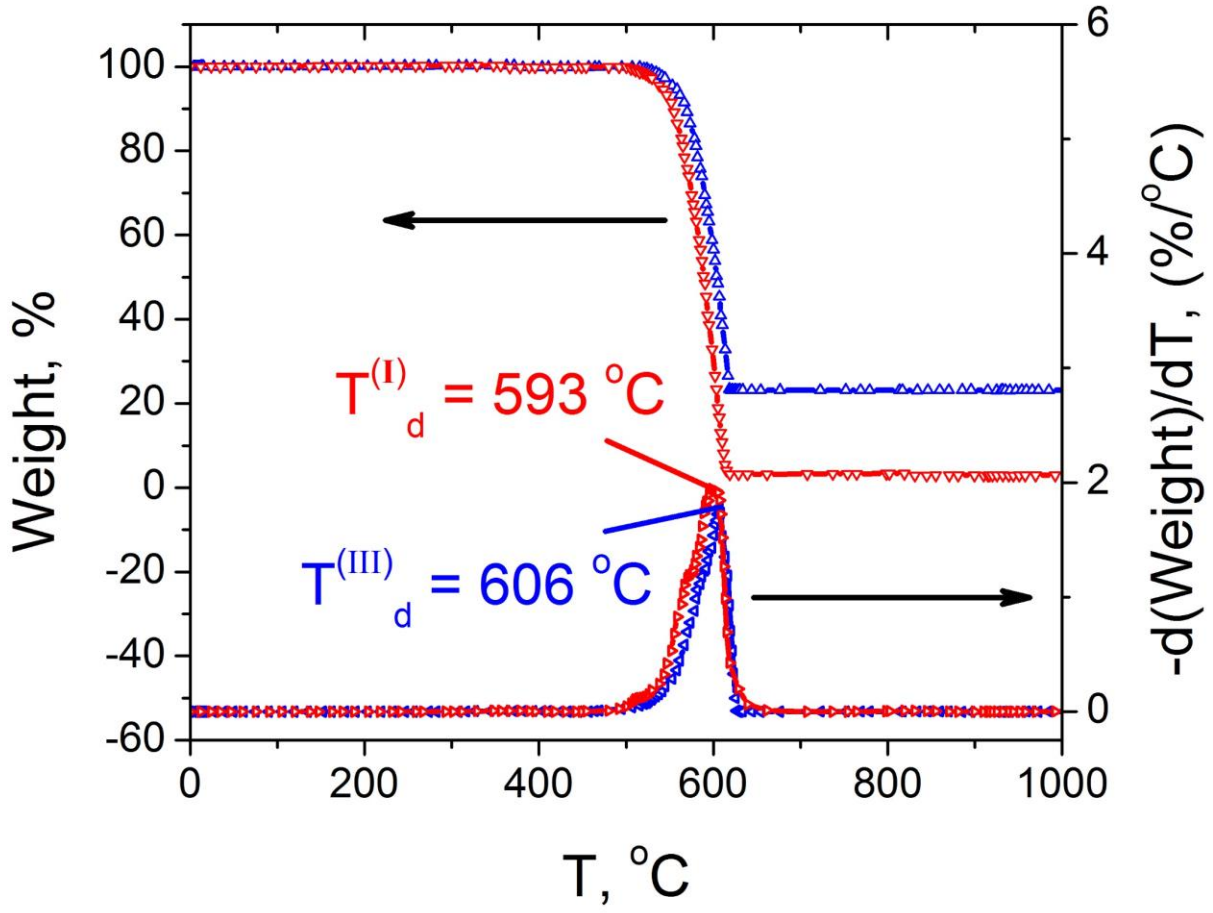

Fig. 12. TGA measurement results for the samples I (red) and III (blue).

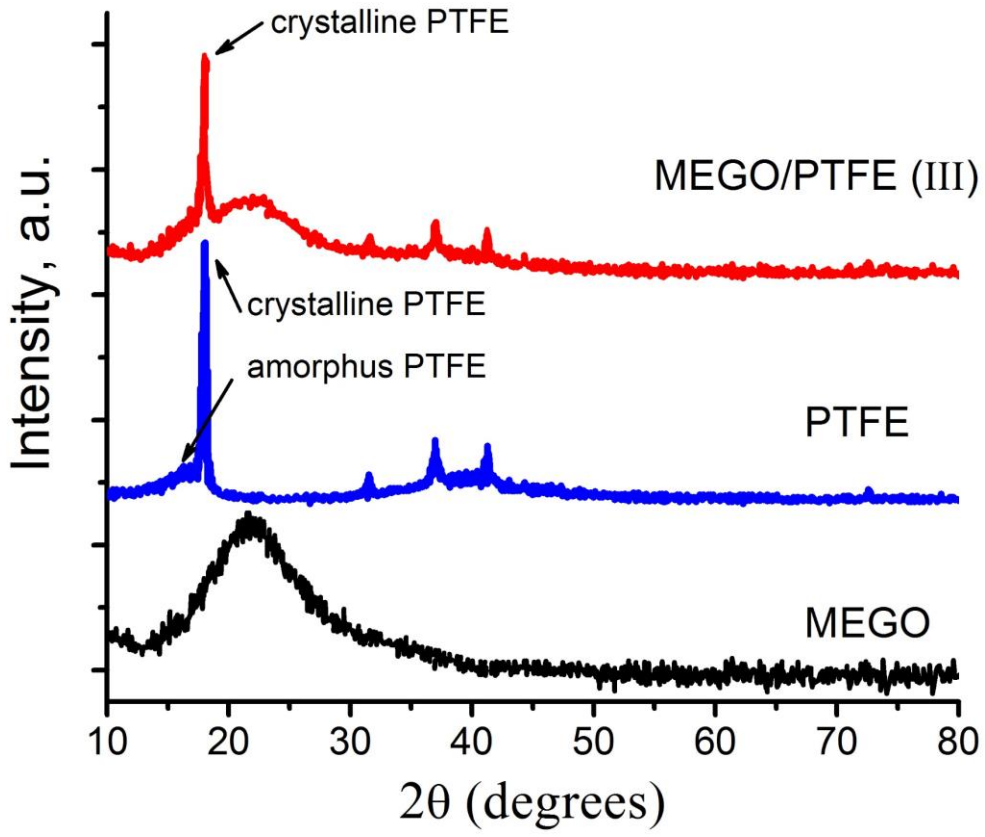

Fig. 13. XRD analysis of MEGO (black), pure PTFE (blue) and MEGO-PTFE (III).

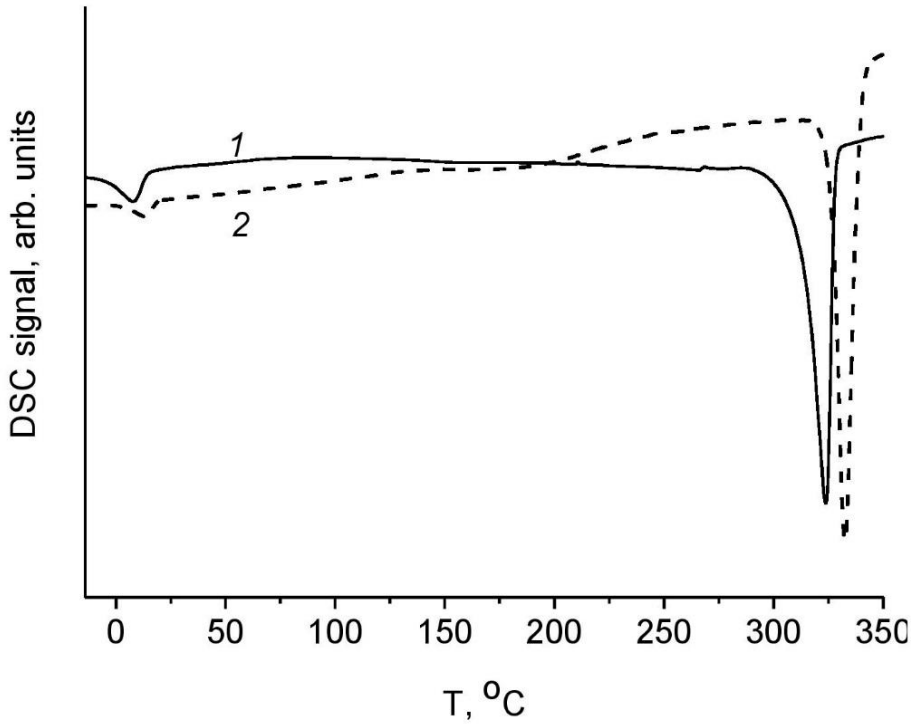

Fig. 14. DSC curves for (1) PTFE and (2) MEGO–PTFE composite 2 (see Table 3).

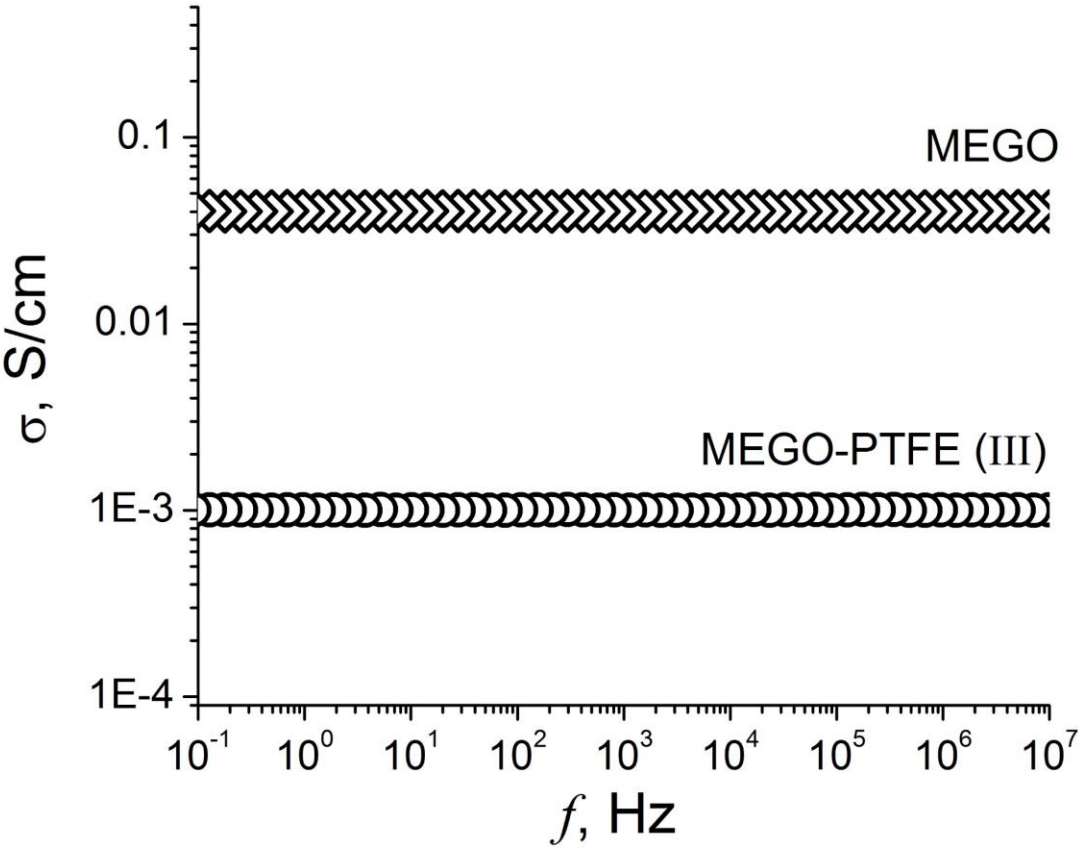

Fig. 15. Conductivity spectrum of MEGO-PTFE (III) (empty circles) and MEGO (empty rhombs) stabilized at room temperature (20 ºC).